Higher-order 1D stick models for the flutter analysis of aircraft structures

HIGHER-ORDER 1D STICK MODELS FOR THE FLUTTER ANALYSIS OF AIRCRAFT STRUCTURES

E. Zappino[1], M. Santori[1], M. Petrolo[1] & E. Carrera[1]

[1]Mul2 Lab, Department of Mechanical and Aerospace Engineering, Politecnico di Torino , Corso Duca degli Abruzzi 24, 10129 Torino, Italy.

Abstract

This paper presents flutter analyses of aircraft structures using an advanced aeroelastic formulation. Three-dimensional problems are reduced to refined 1D structural models based on the Carrera Unified Formulation (CUF). Lagrange expansions of the cross-section displacement field are used. CUF allows for a unified formulation, independent of the type and order of the chosen model, through the use of so-called fundamental nuclei. Aeroelastic results are obtained by coupling the CUF structural model with the doublet-lattice method (DLM). Aeroelastic analyses on thin-wall and multi-component structures are proposed. The advantage of the advanced 1D aeroelastic formulation is that it achieves accuracy comparable to that of 2D plate or 3D solid models while maintaining a low computational cost.

Keywords: Aeroelasticity; Carrera Unified Formulation; aircraft structures; flutter; doublet lattice method.

1. Introduction

The study of aeroelastic phenomena is a crucial aspect of the design of slender structures, particularly in aeronautics. These phenomena emerge due to the interaction between elastic, aerodynamic, and inertial forces in structures that are not completely rigid [1]. Being potentially catastrophic phenomena, it is necessary to predict them through accurate numerical models for even complex structures.

Slender structures can be easily analyzed through 1D structural models, in which the problem variables depend only on the axial coordinate of the beam. Classical Euler-Bernoulli and Timoshenko theories do not allow for nonclassical effects such as torsion-bending coupling or warping. These effects cannot be neglected, for example, in thin-walled structures, particularly in aeroelastic analyses. For this reason, refined beam models have been proposed [2, 3].

In this paper, the 3D structural problem is reduced to a 1D refined structural model, whose variables depend only on the axial coordinate of the beam. The structural models adopted are based on the Carrera Unified Formulation (CUF) [4]. The CUF allows for a unified formulation for which the choice of expansion functions and their order is arbitrary. This formulation was initially developed for plate and shell [5, 6] and then extended to beam [7–9]. CUF-based models can overcome the limitations of classical models. They succeed in detecting, in addition to bending modes, torsional modes in thin-wall [10] structures. In addition, using 1D models enables accurate results and low computational costs compared with 2D and 3D models.

The structural model is coupled with an aerodynamic model for flutter analysis. The doublet lattice method (DLM) was chosen in this work because it offers good accuracy in the subsonic range with competitive computational costs for arbitrary geometries. This method was developed in the 1960s [11] and proposed in an improved version by Rodden [12], introducing a quartic approximation of the oscillatory kernel. In this paper, the DLM implemented in the commercial software MSC NASTRAN is used [13]. The 1D CUF structural model is advantageous for its compatibility with commercial codes. Infinite Plate Spline (IPS) [14] is the interpolation method between structural and aerodynamic models used in MSC NASTRAN [13].

Aeroelastic analyses using the 1D CUF and DLM model of MSC NASTRAN have shown that they can accurately catch flutter phenomena [15]. This paper considers complex thin-wall and whole-aircraft configurations on which free vibration and flutter analyses are carried out.

2. Structural model

A refined one-dimensional structural model based on the Carrera Unified Formulation (CUF) is presented [8]. Next, the CUF will be used to derive the finite element formulation of the governing equations.

2.1 Fundamental equations

Strain and stress vectors are defined as:

$$\boldsymbol{\varepsilon}^T = (\varepsilon_{xx},\ \varepsilon_{yy},\ \varepsilon_{zz},\ \varepsilon_{xz},\ \varepsilon_{yz},\ \varepsilon_{xy}) \tag{1}$$

$$\boldsymbol{\sigma}^T = (\sigma_{xx},\ \sigma_{yy},\ \sigma_{zz},\ \sigma_{xz},\ \sigma_{yz},\ \sigma_{xy}) \tag{2}$$

The strain field $\boldsymbol{\varepsilon}$ can be described through the geometric relation:

$$\boldsymbol{\varepsilon} = \mathbf{D}\mathbf{u} \tag{3}$$

where $\mathbf{D}$ is the differential operator matrix and its explicit expression is given in [16]. $\mathbf{u}$ is the displacement vector.
Hooke's law defines the relationship between the stress vector $\boldsymbol{\sigma}$ and $\boldsymbol{\varepsilon}$:

$$\boldsymbol{\sigma} = \mathbf{C}\boldsymbol{\varepsilon} \tag{4}$$

where $\mathbf{C}$ is the matrix of material coefficients [16].

2.2 Refined one-dimensional model

According to CUF, the displacement field $\mathbf{u}$ for a one-dimensional model is obtained by the following unified formulation:

$$\mathbf{u}(x,y,z) = F_\tau(x,z)\mathbf{u}_\tau(y), \qquad \tau = 1,2,...,M \tag{5}$$

where $\mathbf{u}_\tau$ is the displacement vector, F_τ are the cross-section expanding functions, and τ is an index ranging from 1 to the number of terms in the M expansion. This formulation is independent of the order of the theory, and thus, the choice of F_τ and M is arbitrary. Two different basis functions for modeling the kinematic field on the beam cross-section are considered. Taylor (TE) models use the polynomials $x^m z^n$ where m and n are positive integers. The number of terms in the expansion depends on the order N of the model chosen as input. For example, if a second-order Taylor model ($N = 2$) is chosen, the following parabolic expansion is obtained:

$$\begin{cases} u_x = u_{x_1} + x\,u_{x_2} + z\,u_{x_3} + x^2\,u_{x_4} + xz\,u_{x_5} + z^2\,u_{x_6} \\ u_y = u_{y_1} + x\,u_{y_2} + z\,u_{y_3} + x^2\,u_{y_4} + xz\,u_{y_5} + z^2\,u_{y_6} \\ u_z = u_{z_1} + x\,u_{z_2} + z\,u_{z_3} + x^2\,u_{z_4} + xz\,u_{z_5} + z^2\,u_{z_6} \end{cases} \tag{6}$$

in which there are six generalized displacement variables for each displacement component: one constant, two linear and three parabolic. In Lagrange (LE) models, the expansion functions F_τ coincide with the polynomials of Lagrange. As an example, if a 4-node element (1L4) is used on the cross-section, the expansion functions, written according to the isoparametric formulation, are:

$$F_\tau = \frac{1}{4}(1+\alpha\alpha_\tau)(1+\beta\beta_\tau), \qquad \tau = 1,2,3,4 \tag{7}$$

where α and β denote the normalized coordinates while α_τ and β_τ are the coordinates of the 4 nodes. The field of displacements is:

$$\begin{cases} u_x = F_1\,u_{x_1} + F_2\,u_{x_2} + F_3\,u_{x_3} + F_4\,u_{x_4} \\ u_y = F_1\,u_{y_1} + F_2\,u_{y_2} + F_3\,u_{y_3} + F_4\,u_{y_4} \\ u_z = F_1\,u_{z_1} + F_2\,u_{z_2} + F_3\,u_{z_3} + F_4\,u_{z_4} \end{cases} \tag{8}$$

$u_{x1},...,u_{4z}$ are the displacement variables. Unlike Taylor models, Lagrange models use only the unknowns that make sense from a physical point of view: the displacement components at each node.

2.3 Finite element formulation using CUF

To overcome the limitations of analytical solutions, FEM is used to approximate the displacements along the y axis of the beam. By introducing the shape functions N_i, the range of displacements can be rewritten as:

$$\mathbf{u} = N_i F_\tau \mathbf{q}_{\tau i}, \qquad \tau = 1,2,...,M \quad i = 1,2,...,N_N \tag{9}$$

where $\mathbf{q}_{\tau i}$ is the nodal displacement vector and N_N are the number of nodes along the axis of the beam element.

The Principle of Virtual Displacements (PVDs) is used to obtain the governing equations. Using CUF, the stiffness and mass matrices and the force vector can be written using fundamental nuclei, a unified formulation independent of model type and order.

The virtual work of internal forces is expressed through the PVD as:

$$\begin{aligned} \delta L_{int} = \int_V \delta \boldsymbol{\varepsilon}^T \boldsymbol{\sigma} dV = \\ \delta \mathbf{q}_{\tau i}^{k^T} \left[\int_V \mathbf{D}^T \Big(N_i(y) F_\tau(x,z) \mathbf{I} \Big) \mathbf{C}^k \Big(N_j(y) F_s(x,z) \mathbf{I} \Big) \mathbf{D} dV \right] \delta \mathbf{q}_{sj}^k \end{aligned} \tag{10}$$

which in compact form becomes:

$$\delta L_{int} = \delta \mathbf{q}_{\tau i}^{k^T} \mathbf{k}^{ij\tau s} \delta \mathbf{q}_{sj}^k \tag{11}$$

where $\mathbf{k}^{ij\tau s}$ is the stiffness matrix written in fundamental nuclei form.

To derive the mass matrix according to the unified formulation, we write the work virtual of the inertial forces:

$$\begin{aligned} \delta L_{ine} = \int_V \rho \mathbf{u} \delta \ddot{\mathbf{u}}^T dV = \\ \delta \mathbf{q}_{\tau i}^{k^T} \left[\int_V \rho \Big(N_i(y) F_\tau(x,z) \mathbf{I} \Big) \Big(F_s(x,z) N_j(y) \mathbf{I} \Big) dV \right] \delta \ddot{\mathbf{q}}_{sj}^k \end{aligned} \tag{12}$$

which in compact form is:

$$\delta L_{ine} = \delta \mathbf{q}_{\tau i}^{k^T} \mathbf{m}^{ij\tau s} \delta \ddot{\mathbf{q}}_{sj}^k \tag{13}$$

where $\mathbf{m}^{ij\tau s}$ is the mass matrix in the form of the fundamental nucleus. The components in explicit form $\mathbf{k}^{ij\tau s}$ and $\mathbf{m}^{ij\tau s}$ can be found in Carrera's book [8].

3. Aeroelastic model

In this section, the aerodynamic doublet lattice method (DLM) model is introduced. Then, the spline method to connect the structural and aerodynamic models is presented. Finally, the g-method used to obtain the flutter solution is described.

3.1 Doublet lattice method

The doublet lattice method involves a discretization of the lifting surface into a number of quadrilateral panels. The relationship between the normalwash $\overline{w}$ at the coordinate point x, y and pulsating pressure jump $\overline{\Delta p}$ at the point ξ, η is described by Landahl [17] and Albano [11] and has the following form:

$$\overline{w}(x,y) = \frac{1}{8\pi} \int_A \overline{\Delta p}(\xi,\eta) K(x_0, y_0, \omega, M) dA \tag{14}$$

K the kernel of the complex acceleration potential, the explicit form of which is not given for brevity but can be found in [17]. K depends on the pulsation ω, the Mach number M and the coordinates x_0, y_0 defined as:

$$x_0 = x - \xi; \qquad y_0 = y - \eta \tag{15}$$

Rodden [12] proposed an improved version of the DLM by introducing a quartic approximation of the kernel function. Using Rodden's notation, Eq. 14 becomes:

$$\overline{w}_i = \sum_{j=1}^{N_P} D_{ij} \overline{\Delta p}_j \tag{16}$$

where N_P is the number of aerodynamic panels and D_{ij} is the normalwash factor which is expressed as:

$$D_{ij} = \frac{\Delta x_j}{8\pi} \int_{-e_j}^{e_j} K_{ij}\, d\overline{\eta}_j \tag{17}$$

where Δx_j is the centerline chord of the j-th panel while e_j is half of the length along the η_j direction of the local reference system, of the j-th panel. D_{ij} can be seen as the sum of two contributions, one stationary which is derived from the vortex lattice method (VLM) [18] and one unsteady which is approximated via Rodden's quartic. For brevity, the explicit form of D_{ij} is not shown, but it is described in [12].
The commercial software MSC NASTRAN, used in this work to conduct flutter analysis, uses DLM to define the aerodynamic model.

3.2 The spline method

Infinite Plate Spline (IPS) [14] is the method used to couple the aerodynamic model to the advanced 1D structural model [19]. A grid of fundamental points, called Pseudo-Structural Points, is defined. These points belong to the wing segments, generic trapezoidal aerodynamic surfaces with which the wing surface is divided. At these points, displacements are calculated through the CUF structural model.
As described in [20], we consider a set of motion shapes Φ_m representing the generalized motions for the generation of generalized aerodynamic forces. Slopes and displacements at control and load points of the aerodynamic panels are then given by:

$$\frac{\partial \mathbf{Z}_{m,loc}}{\partial x} = \mathbf{A}_3 \cdot \mathbf{\Phi}_m \tag{18}$$

$$\tilde{\mathbf{Z}}_{m,loc} = \tilde{\mathbf{A}}_3^* \cdot \mathbf{\Phi}_m \tag{19}$$

$$\mathbf{Z}_{m,loc} = \mathbf{A}_3^* \cdot \mathbf{\Phi}_m \tag{20}$$

where $\mathbf{A}_3$, $\tilde{\mathbf{A}}_3^*$ and $\mathbf{A}_3^*$ are obtained via the IPS [14,20]. A case of simply harmonic motion is assumed. The vector of the normalized normal velocities can be expressed through the following relation:

$$\mathbf{w}_m = i\frac{\omega}{V_\infty}\mathbf{Z}_{m,loc} + \frac{\partial \mathbf{Z}_{m,loc}}{\partial x} \tag{21}$$

where i is the imaginary unit. This relationship makes it possible to link the Pseudo-Structural Point displacements calculated through the 1D CUF model and the pressure jumps of the aerodynamic panels obtained from the DLM implemented in MSC NASTRAN [13].

3.3 Generalized matrices and g-method for flutter analysis

The generalized aerodynamic matrix is:

$$\tilde{Q}_{ij}(ik) = \sum_{N=1}^{N_{PA}} \Delta p_j^N(ik)\, \tilde{Z}_{i,loc}^N\, S_{PA}^N \tag{22}$$

where $\Delta p_j^N(ik)$ is the pressure jump from the j-th modal form for a given reduced frequency k and acts on the N-th aerodynamic panel. On the other hand, $\tilde{Z}_{i,loc}^N$ is the i-th set of transverse motions related to the N-th aerodynamic panel, which are mapped onto the aerodynamic panels by the spline method. Finally S_{PA}^N is the area of the aerodynamic panel N.
we denote by $\mathbf{Q}(ik)$ the square matrix of size $N_{modes} \times N_{modes}$, where N_{modes} is the number of natural modes chosen.
The generalized mass matrix is:

$$\tilde{\mathbf{M}} = \mathbf{\Phi}^T \mathbf{M} \mathbf{\Phi} \tag{23}$$

and has dimensions $N_{modes} \times N_{modes}$. $\mathbf{\Phi}$ contains the modal forms and has dimensions $N_{DOF} \times N_{modes}$. N_{DOF} is the total number of DOFs of the structural model. Finally, $\mathbf{M}$ is the mass matrix of dimensions $N_{DOF} \times N_{DOF}$.

The generalized stiffness and damping matrices have the following terms on the diagonal:

$$\tilde{K}_{ii} = \omega_i^2 \tilde{M}_{ii} \tag{24}$$

$$\tilde{C}_{ii} = 2\xi\omega_i \tilde{M}_{ii} \tag{25}$$

where ω_i is the pulsation of the i-th modal form and ξ is the structural damping.
The g-method, described by [21], is used to solve the aeroelastic equation of motion:

$$\mathbf{M}\ddot{\mathbf{x}}(t) + \mathbf{C}\dot{\mathbf{x}}(t) + \mathbf{K}\mathbf{x}(t) = \mathbf{F}(t) \tag{26}$$

where $\mathbf{M}$ is the mass matrix, $\mathbf{C}$ is the damping matrix, $\mathbf{K}$ is the stiffness matrix, $\mathbf{F}$ is the force vector, and $\mathbf{x}$ is the displacement vector. The aeroelastic equation in the Laplace domain can be rewritten by introducing the generalized matrices and the nondimensional Laplace parameter p:

$$\left[\left(\frac{V_\infty}{b}\right)^2 \tilde{\mathbf{M}}p^2 + \frac{V_\infty}{b}\tilde{\mathbf{C}}p + \tilde{\mathbf{K}} - \frac{1}{2}\rho V_\infty^2 \tilde{\mathbf{Q}}(p)\right]\{\mathbf{q}(p)\} = 0 \tag{27}$$

where $p = g + ik$ and $g = \zeta k$, k is the reduced frequency and ζ is transient decay rate coefficient. The parameter b is the reference length, which is usually equal to half the chord. V_∞ is the velocity of the undisturbed flow and ρ is the density of air.
The following approximation of the aerodynamic matrix is assumed:

$$\tilde{\mathbf{Q}}(p) \approx \tilde{\mathbf{Q}}^*(ik) + g\tilde{\mathbf{Q}}^{*'}(ik), \qquad g \ll 1 \tag{28}$$

By substituting Eq. 28 in Eq. 27 the g-method equation is obtained:

$$\left[\left(\frac{V_\infty}{b}\right)^2 \tilde{\mathbf{M}}p^2 + \tilde{\mathbf{K}} - \frac{1}{2}\rho V_\infty^2 \tilde{\mathbf{Q}}^{*'}(ik) - \frac{1}{2}\rho V_\infty^2 \tilde{\mathbf{Q}}^*(ik)\right]\{\mathbf{q}(p)\} = 0 \tag{29}$$

where the contribution of structural damping is neglected.
The generalized aerodynamic matrix $\tilde{\mathbf{Q}}^*(ik)$ is obtained from the DLM in the frequency domain while $\tilde{\mathbf{Q}}^{*'}(ik)$ is obtained numerically.
According to the g-method, solutions that have $Im(g) = 0$ must be found. More details on how to get the solution can be found in [21].

4. Numerical results

In this section flutter analysis on a simple whole aircraft configuration is carried out. The geometric dimensions of the aircraft were taken from [22]. The model has high elongation wings, similar to High-Altitude Long-Endurance (HALE) aircraft. The absence of some model information in [22] prevented a direct comparison of the results. Consequently, an initial analysis focused on the constrained semi-wing, obtaining results with a reasonable level of confidence. Subsequently, these results were compared with those obtained from the entire aircraft with the same constraint. Once the consistency of the results was established, the analysis was extended to the entire unconstrained aircraft.
the wing has a half span $b = 16$ m and chord $c = 1$ m. The rectangular wing is thin-walled and has six ribs along the opening. The thickness of the walls is $h = 0.001$ m and the total thickness of the wing is $a = 0.1$ m. The material of the whole aircraft is isotropic and has the following characteristics: $E = 180$ GPa , $\nu = 0.3$ and $\rho = 1800\,\mathrm{kg/m^3}$. In the analysis, only the semi-wing clamped at the root is considered. The finite element model adopted consists of 21 3-node beam elements (B3). The expansion on the cross section used is 9-node Lagrange type (L9), four elements are used to model the thin-wall section, an additional central one to model the ribs.
The free-vibration analysis of the semi-wing gives as results the frequencies given in Table 1. The results are compared with a plate model created with Femap software (Table 1).

Mode	1D wing frequencies [Hz]	Mode type	2D wing frequencies [Hz]
1	0.5201	I bending around x	0.487
2	2.927	II bending around x	2.749
3	3.387	I bending around z	3.166
4	7.928	III bending around x	7.094
5	17.083	I torsional	14.460
6	18.905	II bending around z	17.805
7	19.490	IV bending around x	19.961

Table 1 – Frequencies related to the first 7 modes of the clamped wing.

Next, the whole aircraft is considered. It consists of a thin-walled tail of the same thickness as the wing and has a half-span equal to $b_t = 2.5$ m and a chord equal to $c_t = 0.5$ m. To model the tail, 7 B3 elements along the beam axis and 4 L9 elements on the cross-section are used. The tail boom connecting the wing and tail has a length of 10 m and a cross-sectional area 0.05 m $\times$ 0.1 m. The adopted FE model consists of 11 B3 elements while only one L9 element is used in the section. The aircraft is constrained in the $y = 0$ along the axis of the tail boom in all directions.
The frequencies and modes obtained from the free-vibration analysis are shown in Table 2 and compared with those obtained for the clamped wing. Given the constraint of the aircraft and the symmetry of the structure, the frequencies are double for each mode. Only one of the two is reported in Table 2.

Mode	1D Aircraft frequencies [Hz]	Mode type	1D wing frequencies [Hz]
1	0.518	I bending around x	0.520
3	2.928	I I bending around x	2.927
5	3.372	I bending around z	3.387
7	7.9001	III bending around x	7.928
9	17.091	I torsional	17.083
11	17.046	I bending around x of the tail	—
13	18.909	II bending around z	18.905
15	19.422	IV bending around x	19.490
DOF	7776		3150

Table 2 – Frequencies of the constrained aircraft and comparison with wing frequencies.

An aerodynamic mesh of 60×8 panels on the wing and 30×4 on the tail is associated with the structural model used for the dynamic analysis in order to perform the flutter analyses. The conditions for which flutter occurs for the wing and the whole aircraft are given in Table 3.

	Speed [m/s]	Frequency [Hz]
Wing	65.507	19.313
Aircraft	68.182	19.495

Table 3 – Flutter conditions for the wing and aircraft constrained in $y = 0$.

The trends of frequencies and damping at varying speed for different modes are shown for the wing and aircraft in Fig. 1 and Fig. 2, respectively.

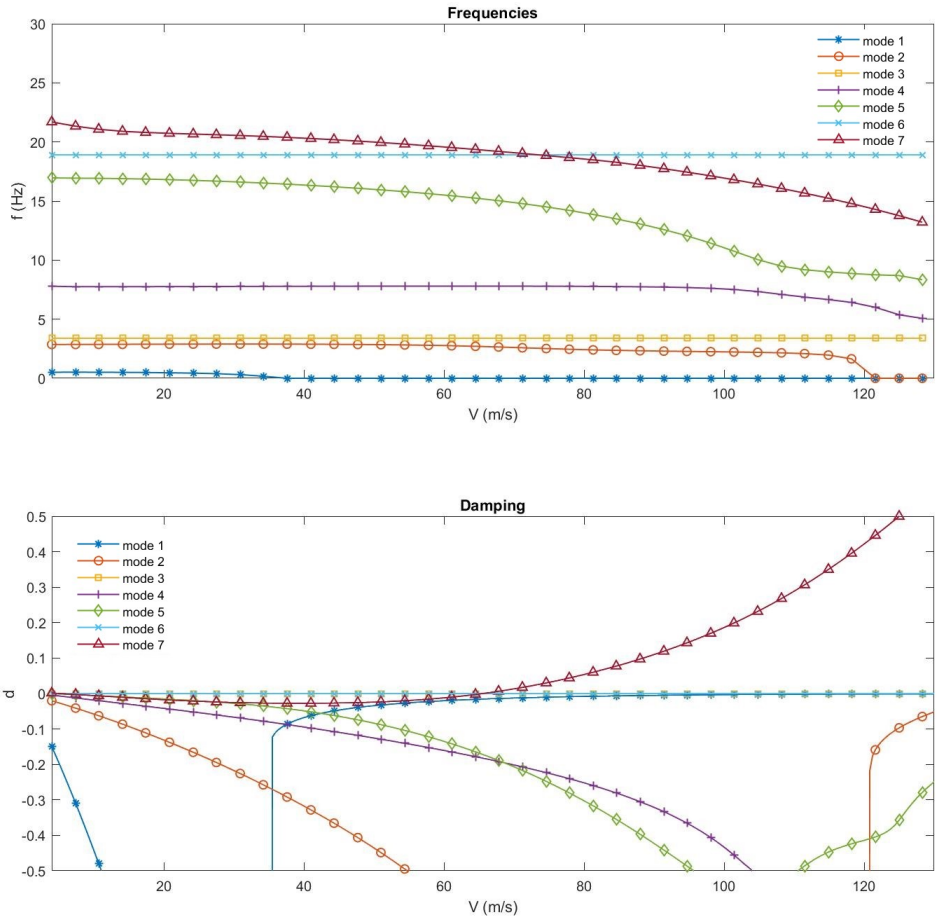

Figure 1 – Frequencies and damping at varying speed for the first 7 modes of the clamped wing.

Finally, the case of a whole aircraft is considered by removing the constraint condition. The frequencies and modes are also calculated for this case (Table 4). Fig. 3 shows the vibrational modes of the aircraft.

Mode	Frequency [Hz]
I bending around x	0.710
II bending around x	1.974
III bending around x	3.823
I bending around z	4.469
IV bending around x	6.461
V bending around x	9.812
I bending around z	13.054
I torsional	16.890
DOF	7776

Table 4 – Frequencies and modes for the aircraft that has no constraints.

While the velocity and frequency for which flutter occurs are given in Table 5. Comparing the results obtained, as the constraint conditions change, the vibration modes and flutter conditions also change. The damping and frequency trends for the unrestrained aircraft case are shown in Fig. 4.

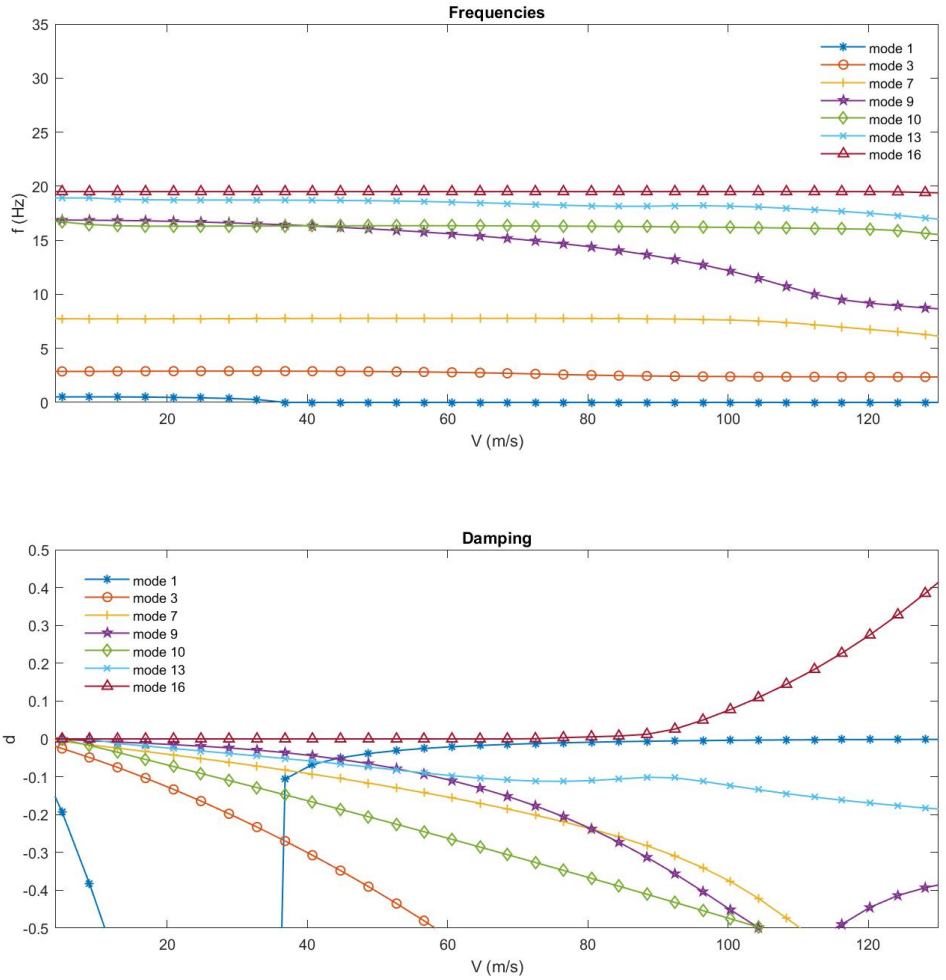

Figure 2 – Frequencies and damping at varying speed for some of the constrained aircraft modes.

Speed [m/s]	Frequency [Hz]
80.139	5.569

Table 5 – Flutter conditions for the unconstrained aircraft.

5. Conclusion

This paper presents flutter analyses in thin-wall wings and simple whole-aircraft configurations. A refined 1D model is coupled with the doublet lattice method to obtain an advanced aeroelastic formulation. Lagrange expansions are used to define the range of displacements in the cross-section.
The free-vibration analyses show that the model based on the Carrera Unified Formulation allows for overcoming the limitations of the classical Euler-Bernoulli and Timoshenko models, being able to predict not only the bending but also the torsional modes correctly of complex structures even in thin walls. This is critical for the correct assessment of flutter conditions. In addition, the refined 1D models used in this work made it possible to analyze complex structures such as aircraft structures accurately and with low computational costs compared to 2D plate or 3D solid models.
In future work, it will be possible to create models with variable kinematics, using Lagrange and Taylor expansions together, so that the number of degrees of freedom can be lowered further without affecting accuracy.

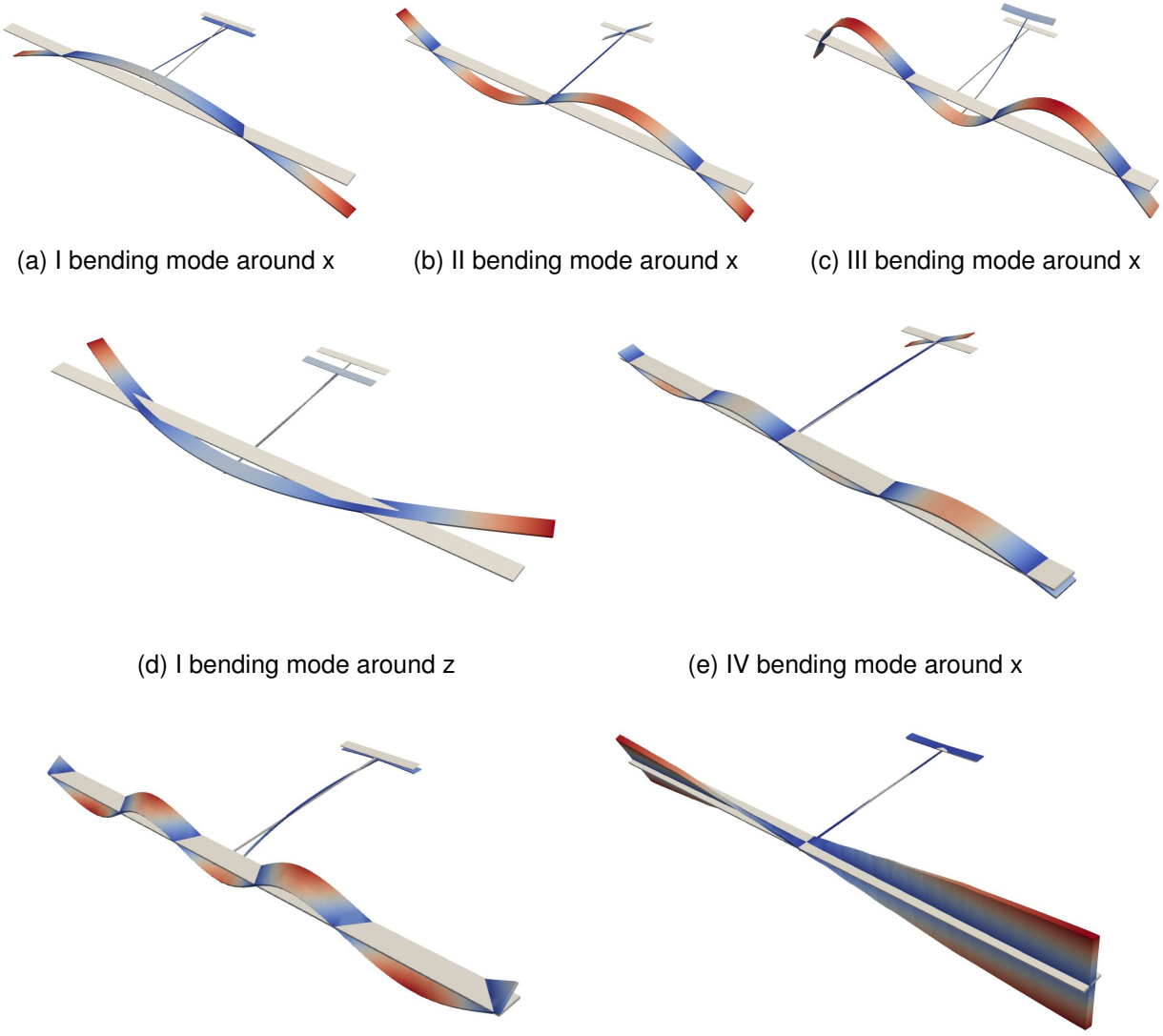

(a) I bending mode around x (b) II bending mode around x (c) III bending mode around x

(d) I bending mode around z (e) IV bending mode around x

(f) V bending mode around x (g) I torsional mode

Figure 3 – Vibrational modes of the unconstrained aircraft.

6. Contact Author Email Address

Mailto: enrico.zappino@polito.it (E. Zappino).

7. Copyright Statement

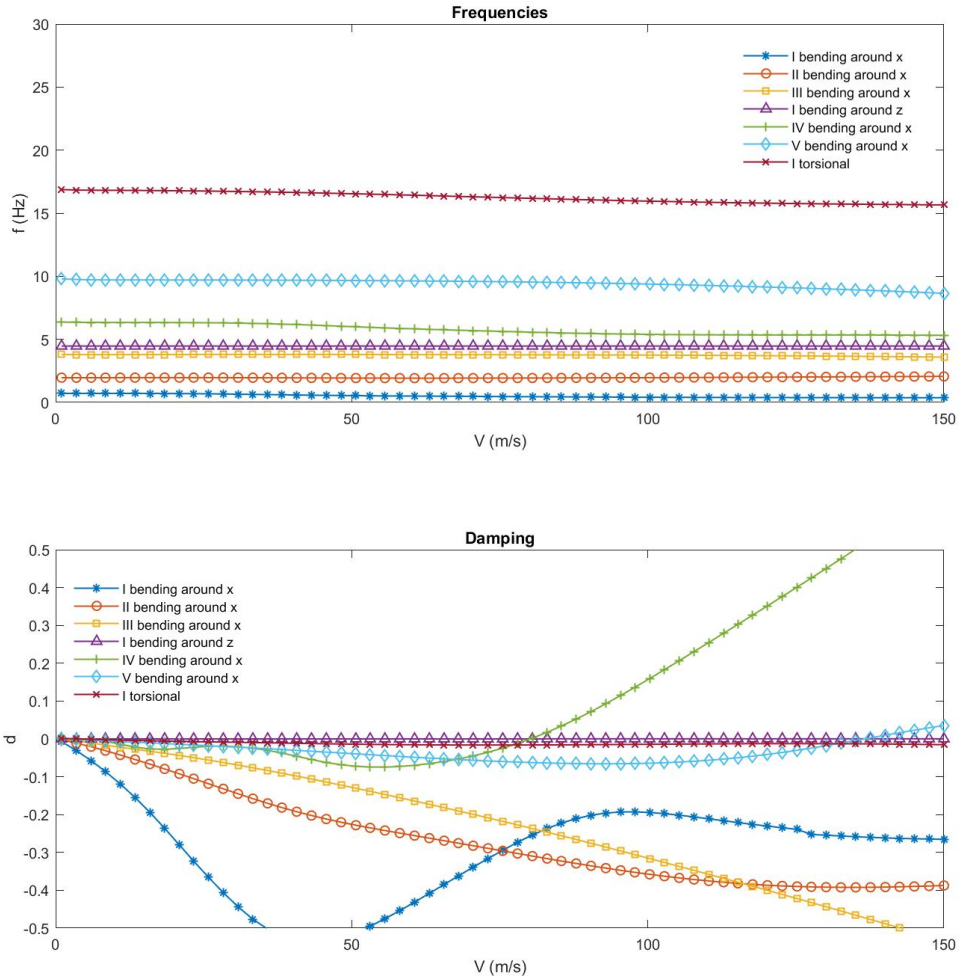

Figure 4 – Frequencies and damping at varying speed for the unconstrained aircraft.

References

[1] Collar, A. R. The expanding domain of aeroelasticity. *The royal aeronautical society*, pp 613–636, 1946.

[2] Librescu, L. and Song, O. On the Static Aeroelastic Tailoring of Composite Aircraft Swept Wings Modelled a Thin-Walled Beam Structures. *Composites Engineering*, Vol. 2(5–7), pp 497–512, 1992.

[3] Reddy, J. On locking-free shear deformable beam finite elements. *Computer methods in applied mechanics and engineering*, Vol. 149(1-4), pp 113-132, 1997.

[4] Carrera, E., Cinefra, M., Petrolo, M. and Zappino, E. Finite element analysis of structures through unified formulation. *John Wiley & Sons*, 2014.

[5] Carrera, E. Theories and finite elements for multilayered anisotropic composite plates and shells. *Archives of computational methods in engineering*, Vol. 9(2), pp 87–140, 2002.

[6] Carrera, E. Theories and finite elements for multilayered plates and shells: a unified compact formulation with numerical assessment and benchmarking. *Archives of Computational Methodsin Engineering*, Vol. 10(3), pp 215-296, 2003.

[7] Carrera, E. and Giunta, G. Refined beam theories based on a unified formulation. *International Journal of Applied Mechanics*, Vol. 2(1), pp 117-143, 2010.

[8] Carrera, E., Cinefra, M., Petrolo, M. et al. Comparisons between 1D (Beam) and 2D (Plate/Shell) Finite Elements to Analyze Thin Walled Structures. *Aerotec. Missili Spaz.* Vol. 93, pp 3–16, 2014.

[9] Nagaraj, M.H., Kaleel, I., Carrera, E. et al. Elastoplastic Micromechanical Analysis of Fiber-Reinforced Composites with Defects. *Aerotec. Missili Spaz.* Vol. 101 , pp 53–59, 2022.

[10] Carrera, E., Petrolo, M., and Nali, P. Unified formulation applied to free vibrations finite element analysis of beams with arbitrary section. *Shock and Vibrations*, Vol. 18(3), pp 485–502, 2011.

[11] Albano, E., Rodden, W. P. A doublet-lattice method for calculating lift distributions on oscillating surfaces in subsonic flows. *AIAA Journal*, Vol. 7(2), pp 279–85, 1969.

[12] Rodden, W. P., Taylor, P. F., and McIntosh, S. C. Further refinement of the subsonic doublet-lattice method. *Journal of Aircraft*, Vol. 35, pp 720–727, 1998.

[13] MSC Nastran. Aeroelastic Analysis User's Guide. 2018.

[14] Harder, R. and Desmarais, R. N. Interpolation using surface splines. *Journal of Aircraft*, Vol. 9(2), pp 189–192, 1972.

[15] Petrolo, M. Flutter analysis of composite lifting surfaces by the 1D Carrera Unified Formulation and the doublet lattice method.*Composite Structures*, Vol. 95, pp 539-546, 2013.

[16] Carrera, E., Giunta, G. and Petrolo, M. Beam structures: classical and advanced theories. *John Wiley & Sons*, 2011.

[17] Landahl, M. T. Kernel function for nonplanar oscillating surfaces in a subsonic flow. *AIAA Journal*, Vol. 5(5), pp 1045–1046, 1967.

[18] Hedman, S. G. Vortex lattice method for calculation of quasi steady state loadings on thin elastic wings in subsonic flow. *FFA*, 1966.

[19] Varello, A., Carrera, E. and Demasi, L. Vortex lattice method coupled with advanced one-dimensional structural models. *Journal of Aeroelasticity and Structural Dynamics*, Vol. 2(2), 2011.

[20] Demasi, L., and Livne, E. Dynamic aeroelasticity of structurally nonlinear configurations using linear modally reduced aerodynamic generalized forces. *AIAA Journal*, Vol. 47(1), pp 71–90, 2009.

[21] Chen, P. C. Damping Perturbation Method for Flutter Solution: The g-Method. textitAIAA Journal, Vol. 38(9), pp 1519–1524, 2000.

[22] Patil, M. J., Hodges, D. H. and Cesnik, C. E. S. Nonlinear aeroelasticity and flight dynamics of high-altitude long-endurance aircraft. *Journal of Aircraft*, Vol. 38, pp 88–94, 2001.